Ultrabroadband 2D electronic spectroscopy with high-speed, shot-to-shot detection

Research Article | Vol. 25, No. 16 | 7 Aug 2017 | OPTICS EXPRESS 18950
Optics EXPRESS

Ultrabroadband 2D electronic spectroscopy with high-speed, shot-to-shot detection

MINJUNG SON, SANDRA MOSQUERA-VÁZQUEZ, AND GABRIELA S. SCHLAU-COHEN*

Department of Chemistry, Massachusetts Institute of Technology, 77 Massachusetts Avenue, Cambridge, MA 02139, USA
*gssc@mit.edu

Abstract: Two-dimensional electronic spectroscopy (2DES) is an incisive tool for disentangling excited state energies and dynamics in the condensed phase by directly mapping out the correlation between excitation and emission frequencies as a function of time. Despite its enhanced frequency resolution, the spectral window of detection is limited to the laser bandwidth, which has often hindered the visualization of full electronic energy relaxation pathways spread over the entire visible region. Here, we describe a high-sensitivity, ultrabroadband 2DES apparatus. We report a new combination of a simple and robust setup for increased spectral bandwidth and shot-to-shot detection. We utilize 8-fs supercontinuum pulses generated by gas filamentation spanning the entire visible region (450 – 800 nm), which allows for a simultaneous interrogation of electronic transitions over a 200-nm bandwidth, and an all-reflective interferometric delay system with angled nanopositioner stages achieves interferometric precision in coherence time control without introducing wavelength-dependent dispersion to the ultrabroadband spectrum. To address deterioration of detection sensitivity due to the inherent instability of ultrabroadband sources, we introduce a 5-kHz shot-to-shot, dual chopping acquisition scheme by combining a high-speed line-scan camera and two optical choppers to remove scatter contributions from the signal. Comparison of 2D spectra acquired by shot-to-shot detection and averaged detection shows a 15-fold improvement in the signal-to-noise ratio. This is the first direct quantification of detection sensitivity on a filamentation-based ultrabroadband 2DES apparatus.

OCIS codes: (300.0300) Spectroscopy; (300.6290) Spectroscopy, four-wave mixing; (300.6300) Spectroscopy, Fourier transforms; (300.6530) Spectroscopy, ultrafast; (300.6629) Supercontinuum generation.

References and links

1. D. M. Jonas, "Two-dimensional femtosecond spectroscopy," Annu. Rev. Phys. Chem. **54**(1), 425–463 (2003).
2. N. S. Ginsberg, Y.-C. Cheng, and G. R. Fleming, "Two-dimensional electronic spectroscopy of molecular aggregates," Acc. Chem. Res. **42**(9), 1352–1363 (2009).
3. F. D. Fuller, J. Pan, A. Gelzinis, V. Butkus, S. S. Senlik, D. E. Wilcox, C. F. Yocum, L. Valkunas, D. Abramavicius, and J. P. Ogilvie, "Vibronic coherence in oxygenic photosynthesis," Nat. Chem. **6**(8), 706–711 (2014).
4. J. Lim, D. Paleček, F. Caycedo-Soler, C. N. Lincoln, J. Prior, H. von Berlepsch, S. F. Huelga, M. B. Plenio, D. Zigmantas, and J. Hauer, "Vibronic origin of long-lived coherence in an artificial molecular light harvester," Nat. Commun. **6**, 7755 (2015).
5. A. A. Bakulin, S. E. Morgan, T. B. Kehoe, M. W. B. Wilson, A. W. Chin, D. Zigmantas, D. Egorova, and A. Rao, "Real-time observation of multiexcitonic states in ultrafast singlet fission using coherent 2D electronic spectroscopy," Nat. Chem. **8**(1), 16–23 (2016).
6. Y.-C. Cheng and G. R. Fleming, "Dynamics of light harvesting in photosynthesis," Annu. Rev. Phys. Chem. **60**, 241–262 (2009).
7. G. S. Schlau-Cohen, A. Ishizaki, and G. R. Fleming, "Two-dimensional electronic spectroscopy and photosynthesis: Fundamentals and applications to photosynthetic light-harvesting," Chem. Phys. **386**(1), 1–22 (2011).
8. J. A. Davis, L. Van Dao, X. Wen, P. Hannaford, V. Coleman, H. Tan, C. Jagadish, K. Koike, S. Sasa, M. Inoue, and M. Yano, "Observation of coherent biexcitons in ZnO/ZnMgO multiple quantum wells at room temperature," Appl. Phys. Lett. **89**(18), 182109 (2006).
9. K. W. Stone, K. Gundogdu, D. B. Turner, X. Li, S. T. Cundiff, and K. A. Nelson, "Two-quantum 2D FT electronic spectroscopy of biexcitons in GaAs quantum wells," Science **324**(5931), 1169–1173 (2009).
10. S. T. Cundiff, T. Zhang, A. D. Bristow, D. Karaiskaj, and X. Dai, "Optical two-dimensional Fourier transform spectroscopy of semiconductor quantum wells," Acc. Chem. Res. **42**(9), 1423–1432 (2009).

#297244 https://doi.org/10.1364/OE.25.018950
Journal © 2017 Received 2 Jun 2017; revised 20 Jul 2017; accepted 21 Jul 2017; published 27 Jul 2017

Optics EXPRESS

11. D. Karaiskaj, A. D. Bristow, L. Yang, X. Dai, R. P. Mirin, S. Mukamel, and S. T. Cundiff, "Two-quantum many-body coherences in two-dimensional Fourier-transform spectra of exciton resonances in semiconductor quantum wells," Phys. Rev. Lett. **104**(11), 117401 (2010).
12. J. Kasprzak and W. Langbein, "Coherent response of individual weakly confined exciton–biexciton systems," J. Opt. Soc. Am. B **29**(7), 1766–1771 (2012).
13. J. R. Caram, H. Zheng, P. D. Dahlberg, B. S. Rolczynski, G. B. Griffin, A. F. Fidler, D. S. Dolzhnikov, D. V. Talapin, and G. S. Engel, "Persistent inter-excitonic quantum coherence in CdSe quantum dots," J. Phys. Chem. Lett. **5**(1), 196–204 (2014).
14. E. Cassette, R. D. Pensack, B. Mahler, and G. D. Scholes, "Room-temperature exciton coherence and dephasing in two-dimensional nanostructures," Nat. Commun. **6**, 6086 (2015).
15. R. D. Mehlenbacher, T. J. McDonough, M. Grechko, M.-Y. Wu, M. S. Arnold, and M. T. Zanni, "Energy transfer pathways in semiconducting carbon nanotubes revealed using two-dimensional white-light spectroscopy," Nat. Commun. **6**, 6732 (2015).
16. J. D. Hybl, A. W. Albrecht, S. M. G. Faeder, and D. M. Jonas, "Two-dimensional electronic spectroscopy," Chem. Phys. Lett. **297**(3), 307–313 (1998).
17. J. D. Hybl, A. Albrecht Ferro, and D. M. Jonas, "Two-dimensional Fourier transform electronic spectroscopy," J. Chem. Phys. **115**(14), 6606–6622 (2001).
18. F. D. Fuller and J. P. Ogilvie, "Experimental implementations of two-dimensional Fourier transform electronic spectroscopy," Annu. Rev. Phys. Chem. **66**, 667–690 (2015).
19. M. L. Cowan, J. P. Ogilvie, and R. J. D. Miller, "Two-dimensional spectroscopy using diffractive optics based phased-locked photon echoes," Chem. Phys. Lett. **386**(1), 184–189 (2004).
20. T. Brixner, T. Mančal, I. V. Stiopkin, and G. R. Fleming, "Phase-stabilized two-dimensional electronic spectroscopy," J. Chem. Phys. **121**(9), 4221–4236 (2004).
21. U. Selig, F. Langhojer, F. Dimler, T. Löhrig, C. Schwarz, B. Gieseking, and T. Brixner, "Inherently phase-stable coherent two-dimensional spectroscopy using only conventional optics," Opt. Lett. **33**(23), 2851–2853 (2008).
22. A. Nemeth, J. Sperling, J. Hauer, H. F. Kauffmann, and F. Milota, "Compact phase-stable design for single-and double-quantum two-dimensional electronic spectroscopy," Opt. Lett. **34**(21), 3301–3303 (2009).
23. E. Harel, A. F. Fidler, and G. S. Engel, "Real-time mapping of electronic structure with single-shot two-dimensional electronic spectroscopy," Proc. Natl. Acad. Sci. USA **107**(38), 16444–16447 (2010).
24. L. A. Bizimana, J. Brazard, W. P. Carbery, T. Gellen, and D. B. Turner, "Resolving molecular vibronic structure using high-sensitivity two-dimensional electronic spectroscopy," J. Chem. Phys. **143**(16), 164203 (2015).
25. N. M. Kearns, R. D. Mehlenbacher, A. C. Jones, and M. T. Zanni, "Broadband 2D electronic spectrometer using white light and pulse shaping: noise and signal evaluation at 1 and 100 kHz," Opt. Express **25**(7), 7869–7883 (2017).
26. T. Wilhelm, J. Piel, and E. Riedle, "Sub-20-fs pulses tunable across the visible from a blue-pumped single-pass noncollinear parametric converter," Opt. Lett. **22**(19), 1494–1496 (1997).
27. H. Zheng, J. R. Caram, P. D. Dahlberg, B. S. Rolczynski, S. Viswanathan, D. S. Dolzhnikov, A. Khadivi, D. V. Talapin, and G. S. Engel, "Dispersion-free continuum two-dimensional electronic spectrometer," Appl. Opt. **53**(9), 1909–1917 (2014).
28. A. Al Haddad, A. Chauvet, J. Ojeda, C. Arrell, F. Van Mourik, G. Auböck, and M. Chergui, "Set-up for broadband Fourier-transform multidimensional electronic spectroscopy," Opt. Lett. **40**(3), 312–315 (2015).
29. B. Spokoyny, C. J. Koh, and E. Harel, "Stable and high-power few cycle supercontinuum for 2D ultrabroadband electronic spectroscopy," Opt. Lett. **40**(6), 1014–1017 (2015).
30. X. Ma, J. Dostál, and T. Brixner, "Broadband 7-fs diffractive-optic-based 2D electronic spectroscopy using hollow-core fiber compression," Opt. Express **24**(18), 20781–20791 (2016).
31. H. Seiler, S. Palato, B. E. Schmidt, and P. Kambhampati, "Simple fiber-based solution for coherent multidimensional spectroscopy in the visible regime," Opt. Lett. **42**(3), 643–646 (2017).
32. R. R. Alfano, *The Supercontinuum Laser Source* (Springer, 2006).
33. M. Bradler, P. Baum, and E. Riedle, "Femtosecond continuum generation in bulk laser host materials with sub-μJ pump pulses," Appl. Phys. B **97**(3), 561–574 (2009).
34. C. Hauri, W. Kornelis, F. Helbing, A. Heinrich, A. Couairon, A. Mysyrowicz, J. Biegert, and U. Keller, "Generation of intense, carrier-envelope phase-locked few-cycle laser pulses through filamentation," Appl. Phys. B **79**(6), 673–677 (2004).
35. F. Hagemann, O. Gause, L. Wöste, and T. Siebert, "Supercontinuum pulse shaping in the few-cycle regime," Opt. Express **21**(5), 5536–5549 (2013).
36. D. Polli, L. Lüer, and G. Cerullo, "High-time-resolution pump-probe system with broadband detection for the study of time-domain vibrational dynamics," Rev. Sci. Instrum. **78**(10), 103108 (2007).
37. F. Kanal, S. Keiber, R. Eck, and T. Brixner, "100-kHz shot-to-shot broadband data acquisition for high-repetition-rate pump–probe spectroscopy," Opt. Express **22**(14), 16965–16975 (2014).
38. J. Brazard, L. A. Bizimana, and D. B. Turner, "Accurate convergence of transient-absorption spectra using pulsed lasers," Rev. Sci. Instrum. **86**(5), 053106 (2015).
39. R. Augulis and D. Zigmantas, "Two-dimensional electronic spectroscopy with double modulation lock-in detection: enhancement of sensitivity and noise resistance," Opt. Express **19**(14), 13126–13133 (2011).
40. I. A. Heisler, R. Moca, F. V. Camargo, and S. R. Meech, "Two-dimensional electronic spectroscopy based on

Optics EXPRESS

conventional optics and fast dual chopper data acquisition," Rev. Sci. Instrum. **85**(6), 063103 (2014).
41. V. Pervak, I. Ahmad, M. K. Trubetskov, A. V. Tikhonravov, and F. Krausz, "Double-angle multilayer mirrors with smooth dispersion characteristics," Opt. Express **17**(10), 7943–7951 (2009).
42. R. Trebino, K. W. DeLong, D. N. Fittinghoff, J. N. Sweetser, M. A. Krumbügel, B. A. Richman, and D. J. Kane, "Measuring ultrashort laser pulses in the time-frequency domain using frequency-resolved optical gating," Rev. Sci. Instrum. **68**(9), 3277–3295 (1997).
43. Y. Zhang, K. Meyer, C. Ott, and T. Pfeifer, "Passively phase-stable, monolithic, all-reflective two-dimensional electronic spectroscopy based on a four-quadrant mirror," Opt. Lett. **38**(3), 356–358 (2013).
44. V. I. Prokhorenko, A. Halpin, and R. J. D. Miller, "Coherently-controlled two-dimensional photon echo electronic spectroscopy," Opt. Express **17**(12), 9764–9779 (2009).
45. A. D. Bristow, D. Karaiskaj, X. Dai, and S. T. Cundiff, "All-optical retrieval of the global phase for two-dimensional Fourier-transform spectroscopy," Opt. Express **16**(22), 18017–18027 (2008).
46. H. L. Fragnito, J.-Y. Bigot, P. C. Becker, and C. V. Shank, "Evolution of the vibronic absorption spectrum in a molecule following impulsive excitation with a 6 fs optical pulse," Chem. Phys. Lett. **160**(2), 101–104 (1989).
47. N. Krebs, I. Pugliesi, J. Hauer, and E. Riedle, "Two-dimensional Fourier transform spectroscopy in the ultraviolet with sub-20 fs pump pulses and 250–720 nm supercontinuum probe," New J. Phys. **15**(8), 085016 (2013).

1. Introduction

Coherent two-dimensional (2D) optical spectroscopy has emerged as a powerful spectroscopic tool for studying the energy landscapes and dynamics of condensed-phase systems [1]. In particular, two-dimensional electronic spectroscopy (2DES), which uses ultrafast visible pulses to excite electronic transitions of the system, has been extensively utilized to unravel couplings between electronic and vibronic states, [2–5] energy relaxation pathways and quantum coherence in a variety of systems including photosynthetic light harvesting complexes [6, 7] as well as organic and inorganic semiconductor nanostructures [8–15]. 2DES has proven to be particularly incisive for interrogating complex systems with highly congested energy states, because time evolution of the third-order signal along one frequency axis (emission frequency, ω_t) is spread out to a second frequency axis (excitation frequency, ω_τ). This grants 2DES a significant advantage over the one-dimensional pump-probe technique: an enhanced spectral resolution while maintaining its ultrafast time resolution.

Since the first demonstration of 2DES technique two decades ago, [16,17] various experimental implementations are actively being developed and examined towards enhanced phase stability, a broader spectral window, and faster data acquisition with improved sensitivity [18]. While early instrumental developments in 2DES were centered on achieving interferometric time precision and phase stability, [19–22] there has recently been a growing interest in the generation of broader excitation sources and development of methods for data acquisition and processing [23–25].

The spectral window of the measured 2D frequency correlation map is directly limited by the bandwidth of the laser spectrum used. Until recently, a non-collinear optical parametric amplifier (NOPA) was the most widely used and accessible source of excitation. Although the wavelength range in a NOPA is readily tunable by varying the phase matching angle, [26] in most cases its bandwidth is limited to sub-100 nm in the visible region, which limits the detection window to a few tens of nanometers in wavelength [18]. This makes NOPA-based apparatuses unable to simultaneously probe the broad range of electronic and vibronic transitions that are typically seen in complex condensed-phase systems, which necessitates the use of a broadband light source to obtain a complete picture of the energy landscape and relaxation pathways. As such, several examples that demonstrate the applicability of few-cycle supercontinuum pulses to 2DES have been reported in recent years [27–31]. While there are several approaches to generate supercontinuum, [32, 33] the most popular method of supercontinuum generation for 2DES is focusing a regenerative amplifier output into a chamber of pressurized argon gas, also known as gas filamentation [34, 35]. Gas filamentation is a simple and robust solution to the drawbacks of white light generation in bulk medium, because it provides $2-3$ orders of magnitude higher pulse energies than those with bulk crystals, and offers a higher damage threshold and lower

Optics EXPRESS

dispersion as no bulk material is present in the medium [33].

However, a major drawback of using ultrabroadband pulses generated by filamentation is that they are inherently less stable than a NOPA output [29]. Thus, high-sensitivity detection that is resistant to the fluctuations of the ultrabroadband source is required. Highly sensitive 2DES enables resolution of weak cross peaks, which may reveal meaningful insights into the dynamics of the system being interrogated, or measurements of photochemically unstable samples or with low pulse energy. Following method developments from transient absorption spectroscopy, [36–38], balanced detection with a reference pulse [24] and shot-to-shot acquisition [25] have been implemented in 2DES, showing a 10-fold and 8.3-fold improvement in sensitivity. While these examples directly show the effect of balanced and shot-to-shot detections on detection sensitivity, the pulses were generated using a NOPA and a YAG crystal, respectively, which are fundamentally different mechanisms with different noise properties from gas filamentation. Although gas filamentation is increasingly being adopted in ultrafast spectroscopy as an alternative to bulk continuum generation, quantitative analysis of the noise profiles and stability of filamentation-based supercontinuum has not been reported. Furthermore, implementation of improved detection methods to offset the instability of the supercontinuum has not yet been demonstrated.

In this work, we present an all-reflective 2D electronic spectrometer that combines an ultrabroadband 8-fs pulse spanning the entire visible region generated by gas filamentation and high-speed, 5-kHz shot-to-shot acquisition. We introduce a dual chopping scheme synchronized to the laser frequency for *in situ* removal of scattered light every shot. Synchronizing the dual chopping scheme with true shot-to-shot detection has not been reported previously, as all previous implementations employ lock-in detection, [39] which is too slow to be synchronized to kHz frequencies, or average several shots for each chopper sequence [30, 40]. This is a simple and robust 2DES setup with only conventional optics that provides a significantly broader spectral window (200 nm) while overcoming the inherent instability of filamentation-based supercontinuum with high-sensitivity detection. We directly quantify the effect of shot-to-shot detection on our supercontinuum pulses, demonstrating a 15-fold improvement compared to conventional, averaged detection. We illustrate the functionality of the setup by measuring the 2D signal of a laser dye, Nile Blue A perchlorate.

2. Experimental details

2.1. Generation and characterization of ultrabroadband pulses

The ultrabroadband excitation source is produced by supercontinuum generation through self-guided argon gas filamentation, as has been reported previously [27, 29]. A 5-kHz Ti:sapphire regenerative amplifier (Coherent Libra) provides the initial input pulses that are centered at 800 nm (32-nm bandwidth) with a pulse duration of less than 40 fs. To generate the supercontinuum, an attenuated output of the regenerative amplifier is focused into a 1-m long steel chamber filled with pressurized argon gas at 20 psi. Typically, a minimum pulse energy of 540 μJ was required to initiate the supercontinuum generation. The resultant spectrum exhibits spectral broadening around the center wavelength of the fundamental (inset of Fig. 1(c)), although the intensity at wavelengths shorter than 700 nm is nearly three orders of magnitude lower than that around 800 nm. To attenuate the intense residual from the fundamental, the initially broadened pulse is collimated and passed through a shortpass dichroic mirror with a cutoff wavelength of 805 nm (Thorlabs), and then two colored glass bandpass filters with transmittance at 330 – 665 nm. Figure 1(c) shows the spectrum of the final output pulse, which spans the entire visible region (450 – 800 nm) with a full-width at half maximum (FWHM) bandwidth of 180 nm centered at 575 nm. The energy of the pulse after all spectral filtering is 12 μJ.

The shot-to-shot intensity fluctuation of the ultrabroadband pulse was measured by recording 1024 consecutive spectra at 5 kHz, and revealed a relative standard deviation (RSD) of 1.5% in the integrated intensity and 1.3% at 580 nm, respectively. The long-term stability was also

Optics EXPRESS

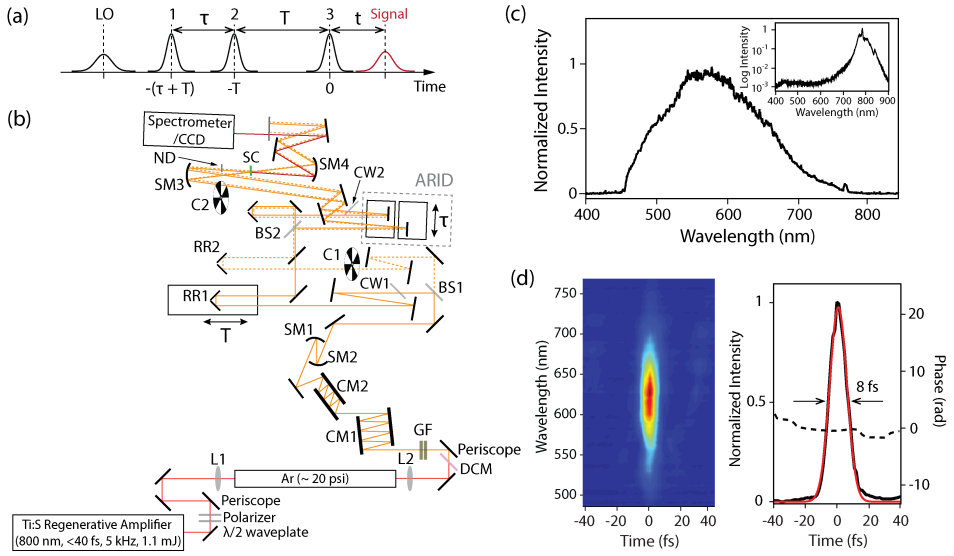

Fig. 1. (a) Pulse sequence of a 2DES experiment. Time zero is arbitrarily set to the point where pulses 1 – 3 are coincident on the sample. The local oscillator (LO) is temporally delayed to precede the other three pulses to prevent pump-probe background from interfering with 2D signal. (b) Optical layout of the ultrabroadband 2DES setup. L1 and L2 – focusing and collimating lenses (f = 1000 mm); DCM – shortpass dichroic mirror (805 nm cutoff); GF – glass filters; CM1 and CM2 – chirped mirror pairs; SM1 and SM2 – spherical (concave) mirrors (f = 150 mm and 75 mm); SM3 and SM4 – spherical (concave) mirrors (f = 250 mm); BS1 and BS2 – 50:50 beam splitters; CW1 and CW2 – compensating windows (1-mm UV fused silica); RR1 and RR2 – retroreflectors; C1 and C2 – optical choppers; ND – neutral density filter (OD 3); SC – sample cell. The all-reflective interferometric delay (ARID) assembly is marked with a gray, dashed box. (c) Spectrum of the ultrabroadband light source measured after spectral filtering. Inset shows the initial broadened spectrum before filtering. (d) Left: TG-FROG trace of the ultrabroadband pulse measured at the sample position. Right: Temporal intensity (black solid line) fitted with a Gaussian function (red) and phase (black dashed line) profiles retrieved from FROG. The pulse FWHM was measured to be 8 fs.

examined by collecting the spectrum every 30 seconds over 4 hours, and we observed an intensity fluctuation of 2.0% and a spectral fluctuation of 1.7% at 580 nm. This is comparable to the fluctuation of the input beam, with an RSD of 1.7% for the intensity fluctuation and 1.3% measured at 800 nm. This indicates that the intensity fluctuation of the ultrabroadband pulse is dominated by the shot noise, and there is no long-term drift in the intensity.

The pulse is compressed with two pairs of group velocity delay (GVD)-oscillation-compensated chirped mirrors (CM1 and CM2, Ultrafast Innovations) with an average GVD of -40 fs^2/mm per double bounce [41]. A variable amount of UV fused silica (1–2 mm) is used for fine tuning of the dispersion. The temporal profile of the pulse is characterized by measuring transient grating frequency-resolved optical gating (TG-FROG) [42] on a 5-mm thick N-BK7 glass at the sample position with a 200-nJ pulse energy (Fig. 1(d)). The TG-FROG trace shows that the entire spectrum of the ultrabroadband pulse is compressed to a FWHM of 8 fs. Finally, the beam diameter of the compressed pulse is reduced from 6 mm to 3 mm using two concave mirrors (SM1 and SM2, Newport), and the 3-mm beam is sent into the all-reflective 2DES setup.

Optics EXPRESS

2.2. All-reflective, fully non-collinear two-dimensional electronic spectrometer

The optical layout of the all-reflective 2DES setup is shown in Fig. 1(b). To minimize any further wavelength-dependent dispersion, no transmissive optics were used throughout the system with the exception of two UV fused silica compensating windows (CW1 and CW2) and two 1-mm thick ultrafast beam splitters (Layertec), which create four beams in a fully non-collinear, BOXCARS phase-matching geometry. The first beam splitter (BS1) creates a vertical separation between pulse pairs 1 – 2 and 3 – LO. The second beam splitter (BS2) then separates the two pairs horizontally, which results in a 0.5 inch × 0.5 inch BOXCARS geometry. The waiting time (T) is introduced by temporally delaying beams 1 and 2 from beam 3 and the LO by a retroreflector (RR1) mounted on a motorized translational stage (Aerotech).

Because 2DES is a Fourier-transform spectroscopic technique, it is critical to ensure an interferometric precision in the timing between pulses. For example, timing jitters as small as 0.5 fs will lead to peaks appearing at incorrect frequencies in the ω_τ domain, or cause ghost peaks to appear [1, 18]. To control the coherence time (τ) with interferometric precision but without introducing further dispersion, we have adopted the all-reflective interferometric delay (ARID) system reported by Zheng et al (Fig. 2) [27]. The system consists of four independent square mirrors arranged in a four-quadrant fashion [43]. Of the four, the bottom two mirrors, which reflect beams 1 and 2, are mounted and translated on two mechanical stages at a small angle (~0.3°) to the plane normal to the beam propagation. In this geometry, the effective increment (Δx) in τ is greatly reduced from the actual increment of the translational stage (Δd) when θ is small ($\Delta x = \Delta d \sin\theta$) [27]. This gives us a much more precise control over the coherence time steps without approaching the mechanical limit of the precision of the stage (in our case, 100 nm). For example, moving the nanopositioners in 100-nm steps at the chosen angle (0.3°) leads to a minimum Δx of 0.524 nm, which corresponds to 1.75 as in time.

In our system, the two bottom mirrors are mounted on two motorized nanopositioners (Aerotech), which are then mounted on a base plate with screw holes at variable positions so that the angle (θ) can be readily varied without having to unmount the individual optical components. Of the two top mirrors, one mirror (M_{LO}) is mounted on a manual linear stage to introduce a temporal delay to the LO from the other three beams. In the BOXCARS geometry, the rephasing ($k_R = -k_1 + k_2 + k_3$) and non-rephasing ($k_{NR} = k_1 - k_2 + k_3$) contributions of the signal are collected separately by reversing the timing between pulses 1 and 2. Specifically, at any given waiting time T, beam 1 is scanned from $-(\tau + T)$ to $-T$ for the rephasing pathways, and beam 2 is swept from $-T$ to $-(\tau + T)$ to obtain the non-rephasing spectra by moving the corresponding nanopositioners (see Fig. 1(a) for the pulse sequence of a 2DES measurement).

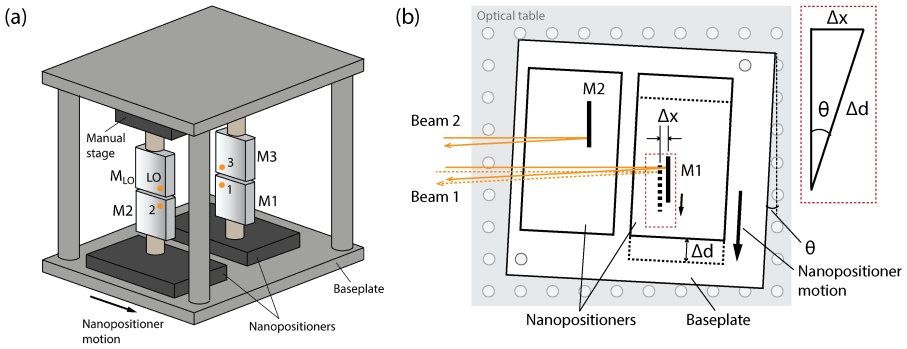

Fig. 2. Schematic of the ARID assembly. (a) Side view and (b) top view. The top two mirrors and the top plate are omitted for clarity.

Optics EXPRESS

The wavelength-dependent calibration factor ($\Delta x/\Delta d$) is empirically determined by recording the spectral interferogram between beams 1 and 2 by scanning each nanopositioner. From the obtained interferogram, we take slices at several different wavelengths and fit the oscillatory traces to a sinusoidal curve to calculate the calibration factor. At the angle employed in our system ($\theta = \sim 0.3°$), the fits consistently gave us a ($\Delta x/\Delta d$) of 45 fs/mm irrespective of the wavelength probed, which is approximately a 150-fold improvement in precision compared to 6673 fs/mm using a retroreflector ($\theta = 90°$). Furthermore, the all-reflective nature of this design is particularly well-suited for a broadband 2DES setup because it is free from wavelength-dependent dispersion, which can be an issue when using wedge pairs [18]. The angle θ can also be adjusted to a larger value to probe a longer range of coherence times at the cost of precision.

In addition to ensuring an interferometric precision in coherence time delays, maintaining phase stability is another critical experimental consideration in 2DES. A commonly used method to achieve phase stability is to design a (near-)common-path instrument by using common optics for all four beams. This method takes advantage of the fact that the phase fluctuations between pulse pairs 1 – 2 and 3 – LO are anti-correlated [19, 44]. In the case of the rephasing pathway ($k_R = -k_1 + k_2 + k_3$), the heterodyne-detected third-order signal (S_R) can be written as

$$S_R(\omega) = \hat{\chi}^{(3)}(\omega_R; \omega_1, \omega_2, \omega_3)|E(\omega)|^4 e^{-i\omega(-t_1+t_2+t_3-t_{LO})} e^{i\omega(-\varphi_1+\varphi_2+\varphi_3-\varphi_{LO})}, \quad (1)$$

where $\hat{\chi}^{(3)}$ is the third-order nonlinear susceptibility, ω_R is the frequency of the rephasing 2D signal, $E(\omega)$ is the electric field, t_i and φ_i are the delay and phase of the ith pulse [45]. Thus, the total phase of the rephasing signal (φ_R) is

$$\varphi_R = -i\omega(-t_1 + t_2 + t_3 - t_{LO}) + i\omega(-\varphi_1 + \varphi_2 + \varphi_3 - \varphi_{LO}). \quad (2)$$

Because the first term is measured during the 2DES experiment and can be removed, the phase offset of the signal from the incident pulses ($\Delta\varphi_R$) can be written as

$$\Delta\varphi_R = -\varphi_1 + \varphi_2 + \varphi_3 - \varphi_{LO} = (\varphi_2 - \varphi_1) + (\varphi_3 - \varphi_{LO}). \quad (3)$$

The overall phase fluctuation that the signal experiences ($\delta(\Delta\varphi_R)$) can then be written as [44]

$$\delta(\Delta\varphi_R) = (\delta\varphi_2 - \delta\varphi_1) + (\delta\varphi_3 - \delta\varphi_{LO}). \quad (4)$$

Therefore, phase stability is achieved in a 2DES apparatus that uses common paths to generate the four beams, because the two terms cancel out even if the individual terms are non-zero [19,44]. Our 2DES setup also relies on this passive phase stabilization method, but because the ARID has separate mirrors for each beam, the phase fluctuations between the two pulse pairs are not strictly anti-correlated. Each phase fluctuation term ($\delta\varphi_i$) in Eq. (4) can be explicitly written out as the sum of the fluctuation originating from each optic in the beam path. Eventually, all other terms cancel out between the pulse pairs 1 – 2 and 3 – LO, and the overall phase fluctuation of the rephasing signal consists of only four terms that correspond to the phase fluctuation of the four mirrors in the ARID system:

$$\delta(\Delta\varphi_R) = (\delta\varphi_{M2} - \delta\varphi_{M1}) + (\delta\varphi_{M3} - \delta\varphi_{M_{LO}}). \quad (5)$$

To minimize the above-mentioned phase fluctuation from the mirrors, the entire ARID system was constructed with steel, and steel mounts were used for all optics. The phase stability of the setup was measured by recording the interferogram between beams 1 and 2 at fixed stage positions (Fig. 3(a)). The standard deviation (σ) of the phase retrieved from the interferogram at the center wavelength of the ultrabroadband pulse (575 nm) was 43 mrad over 20 minutes and 84 mrad over 10 hours, which corresponds to the short-term and long-term phase stability of $\lambda/146$ (20 minutes) and $\lambda/75$ (10 hours), respectively (Fig. 3(b)). Figure 3(c) shows that the spectral

Optics EXPRESS

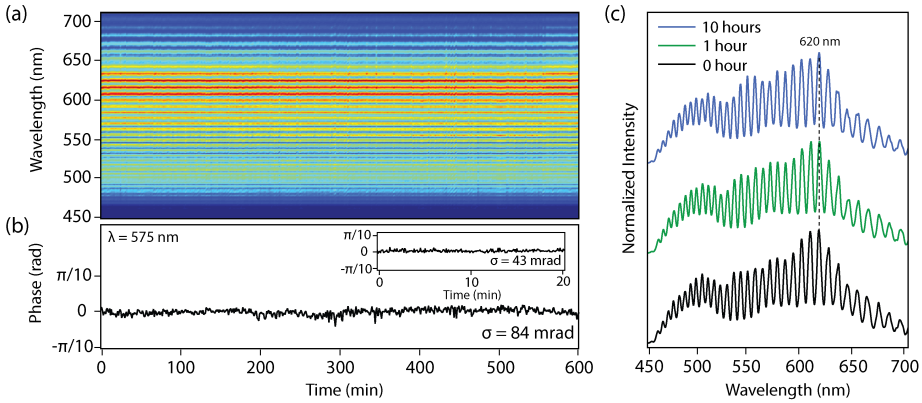

Fig. 3. (a) Spectral interferogram of beams 1 and 2 measured every minute over 10 hours. (b) Phase retrieved from the spectral interferogram at 575 nm. The long-term standard deviation (σ) of the phase is 84 mrad, corresponding to a long-term phase stability of $\sim\lambda/75$. Inset: Short-term phase stability measured every 20 seconds over 20 minutes. (c) Time slices of the spectral interferogram (displayed with vertical offset for clarity). The middle (green) and the top (blue) spectra were recorded one hour and 10 hours after the bottom spectrum (black), respectively. A vertical dashed line at 620 nm is shown as a guide to the eye.

interferograms measured after one hour and after 10 hours are in phase with the one measured first, which confirms that our setup is phase-locked.

After the four beams are reflected off the mirrors in the ARID assembly, they are focused to a 100-μm diameter spot on the sample with a concave mirror (f = 250 mm, Newport). The LO is attenuated by three orders of magnitude before entering the sample and temporally delayed by ~500 fs by translating M_{LO} on a linear stage (see Fig. 2(a)), such that it enters the sample before beams 1 – 3. After recollimation, a spatial mask blocks beams 1 – 3 to prevent scattered light from going into the detection system. Finally, the heterodyned signal is sent into a home-built spectrometer, in which a volume phase holographic grating (450 grooves/mm, Wasatch Photonics) spectrally disperses the signal and focuses it into a 1 × 2048 pixel line-scan CCD (e2v Aviiva EM4-BA8). The spectral resolution of the spectrometer is 0.145 nm/pixel, and a typical detection range of the emission frequency (ω_t) is 470 – 770 nm.

2.3. *Shot-to-shot data acquisition and scatter removal*

In our detection system, we have introduced a high-speed, shot-to-shot (5-kHz) data acquisition scheme to enhance the sensitivity of the measurement while reducing the data acquisition time. Furthermore, we employ two optical choppers (C1 and C2) that operate at subharmonics of the laser frequency to subtract scatter contributions from the raw data, which is known to be a major source of background in 2DES [39].

Figure 4(a) illustrates the connectivity diagram of the electronic components in our detection system. Here, the two optical choppers, which operate at 2.5 kHz (C1) and 1.25 kHz (C2), respectively, are synchronized to the 5-kHz output signal from the synchronization and delay generator (SDG) of our laser. C1 chops beams 1 and 2, and C2 chops beam 3 as shown in Fig. 4(b). This dual chopping leads to a unique sequence of four different combinations of pulses, which are marked A – D in the figure. A tailor-made data acquisition software calculates A–B–C+D, which gives the scatter-subtracted 2D signal at each τ at a given T [20, 40]. To circumvent the issue of conventional electronics being too slow for a 5-kHz detection, we employ a microcontroller (Arduino mega) and a high-speed, line-scan CCD that can operate at a frequency as high as 70

Optics EXPRESS

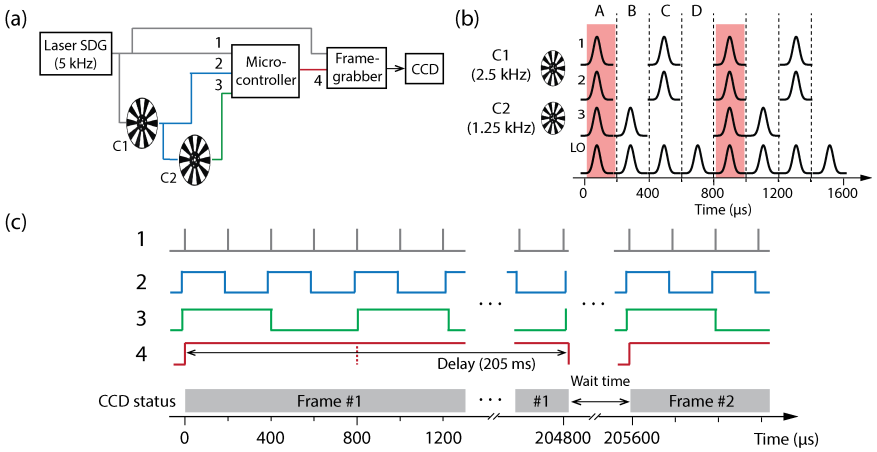

Fig. 4. (a) Schematic drawing of the hardware in the detection part. The TTL output signals of our laser (1) and two choppers (2, 3) serve as a trigger input of the microcontroller. The microcontroller output (4) is wired to the frame grabber input port, which receives the AND gate signal from the microcontroller and triggers data acquisition. (b) Illustration of dual chopping. 2D signal is emitted only in the shaded parts of the sequence, where beams 1–3 are all unblocked. (c) Electronic input/output signals of each hardware component as marked in (a) and their synchronization with CCD acquisition. Wait time denotes the interval between frames when no image acquisition occurs. This ensures that every frame acquisition is synchronized to the pulse sequence A – D in the correct order.

kHz. The microcontroller is synchronized by taking the transistor-transistor-logic (TTL) output signal from the laser (1) and the two choppers (2 and 3) such that its TTL output 4 becomes high only if all inputs 1–3 are high, which serves as the trigger for data acquisition. Because our frame grabber can acquire up to 1024 consecutive lines before transferring the data to the computer, we define 1024 lines × 2048 pixels as our unit array of data acquisition ("frame"). Thus, it takes (1024 lines) / (5000 lines/s) = 204.8 ms to collect each frame, which contains 256 pulse sequences A – D recorded every laser shot. For frame-by-frame acquisition as described above, we program a delay time that is slightly greater than 204.8 ms (205 ms) into the microcontroller so that the AND gate signal stays high for 1024 triggers regardless of the chopping sequence. After this time, the AND gate signal returns to low and waits for the next A sequence (all beams unblocked) to initiate the collection of the next frame (Fig. 4(c)).

3. Ultrabroadband two-dimensional electronic spectroscopy

To demonstrate the functionality of our setup, Nile Blue A perchlorate dissolved in ethanol was chosen as a test sample. The experiment was carried out with a pulse energy of 7 nJ/pulse in a 0.1-mm thick quartz cuvette with an optical density of 0.2 at the absorption maximum (628 nm). The coherence time (τ) was incremented by 0.4 fs over a range of -100 to 100 fs, and the waiting time (T) was sampled every 5 fs from 0 to 600 fs.

Figure 5(a) shows an example 2D spectrum of Nile Blue at T = 200 fs, which shows a ground-state bleach (GSB) peak of the dye along the diagonal at the absorption maximum. To separate out the real and imaginary parts of the signal, the 2D amplitude spectrum was phased using the projection slice theorem [1]. Auxiliary pump-probe spectra of the dye were measured by blocking beams 1 and 3 and using beam 2 as the pump and LO as the probe. The projection of the real part of the raw 2D spectrum onto the ω_t axis ($S_{2D}(\omega_\tau, T, \omega_t)$) was multiplied by a

Optics EXPRESS

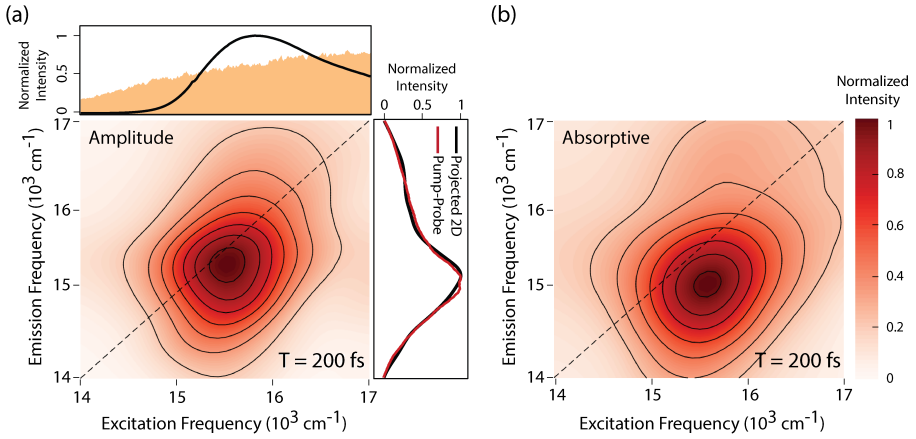

Fig. 5. (a) 2D amplitude spectrum of Nile Blue A perchlorate at a waiting time (T) of 200 fs. The overlay of the laser spectrum (shaded orange area) with the dye linear absorption (black line) is shown above the 2D spectrum. On the right, we plot the pump-probe (red) and the projected 2D spectrum (black) phased using the pump-probe spectrum. (b) Real (absorptive) 2D spectrum of Nile Blue A perchlorate after phasing.

series of phase factors until it matched the normalized pump-probe spectrum $PP(T,\omega_t)$:

$$PP(T,\omega_t) = Re\left\{\int_{-\infty}^{\infty} S_{2D}(\omega_\tau,T,\omega_t)exp\left(i(\phi+(\omega_t-\omega_0)t_c+(\omega_t-\omega_0)^2t_q^2+(\omega_\tau-\omega_0)\tau_c)\right)d\omega_\tau\right\}, \tag{6}$$

where ω_0 is the laser center frequency [13]. Here, we use four different phase factors to phase the 2D spectrum: ϕ is an overall constant phase correction, t_c and t_q correct the linear and quadratic errors in the time delay between beam 3 and the LO, and τ_c is the correction term for the drift in $\tau = 0$. In most cases the last term (τ_c) was not needed, which confirms the phase stability of our setup.

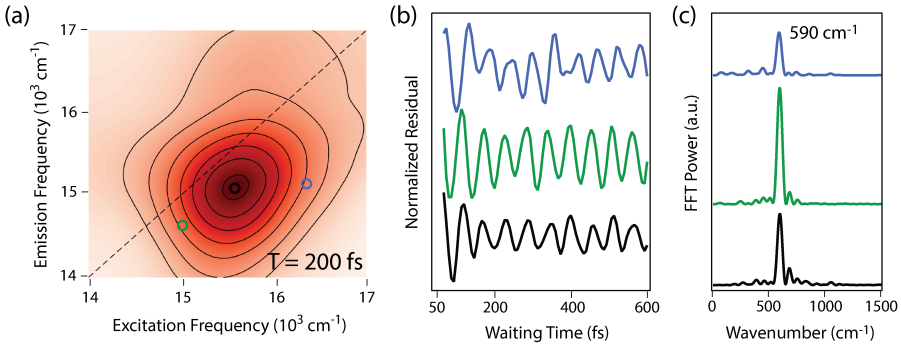

Fig. 6. (a) Absorptive 2D spectrum of Nile Blue A perchlorate at T = 200 fs. The open circles indicate the three points monitored for oscillations in waiting time dynamics. (ω_τ, ω_t) = (16300 cm^{-1}, 15100 cm^{-1}) (blue); (15000 cm^{-1}, 14500 cm^{-1}) (green); (15600 cm^{-1}, 15000 cm^{-1}) (black). (b) Plot of oscillations along waiting time observed at the three exemplary points marked in (a). (c) Fourier-transformed power spectra of the oscillations in (b).

Optics EXPRESS

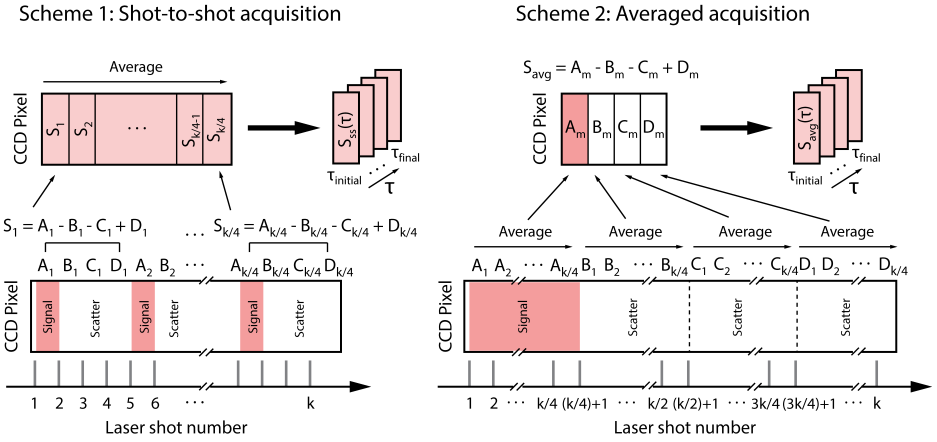

Fig. 7. Schematic illustration of the shot-to-shot and averaged data acquisition schemes for k consecutive laser shots.

Figure 5(b) is the plot of the real (absorptive) part of the 2D spectrum, which shows very little difference from the amplitude spectrum except for a slight frequency shift along the ω_t axis. This indicates that the 2D signal of Nile Blue is dominated by the GSB contribution, in agreement with previously reported results [20, 31]. The 2D signal intensity plotted along T reveals strong oscillations superimposed to the population dynamics, which originate from vibrational wave packet motions of Nile Blue [31, 46]. To separate out the wave packet motion from population dynamics, we subtract the exponential decay component from the modulated 2D intensity traces and Fourier transform the residuals (Fig. 6(b),(c)). At three different frequencies probed, we consistently get a frequency of 590 cm^{-1}, which is known to correspond to the ring distortion mode of Nile Blue [46].

4. Comparison between shot-to-shot and averaged data acquisition

In this section, we compare the sensitivity of our 5-kHz shot-to-shot acquisition and the traditional, averaged acquisition schemes. Figure 7 summarizes the two different data acquisition mechanisms. Scheme 1 is the shot-to-shot acquisition scheme that we described earlier. Every shot, we sequentially collect the four pulse combinations A – D (Fig. 4(b)), construct the scatter-subtracted data arrays ($S_{k/4}$) with four adjacent shots, and average them to get the final data block S_{SS} for each τ. On the other hand, in the averaged acquisition scheme (Scheme 2), which is commonly used in shutter-based 2DES setups, [20] each of the four different pulse combinations A – D is recorded in blocks for $(k/4)$ consecutive shots and averaged $(A_m - D_m)$, instead of alternating the four cases every shot. Scatter-subtracted data arrays (S_{avg}) are obtained after collecting all k shots.

We have directly compared the signal-to-noise ratio (SNR) of these two acquisition schemes by evaluating the noise level of the raw interferogram in the τ domain (Fig. 8). Each 2D spectrum presented here is an average of 1024 laser shots. Differences are observed in both the processed 2D spectra and the interferograms in the τ domain. Although the position of the main peak is not changed, the 2D spectrum acquired by Scheme 2 exhibits spurious structures in the peak. These structures are not observed in the 2D spectrum acquired shot by shot, which suggests that they are artifacts caused by noise. To quantify the SNR, we compare the normalized τ domain data in a range of 0 to 100 fs at two different emission frequencies (ω_t), 15500 cm^{-1} and 16600 cm^{-1}. Following a previously established analysis method, [25, 47] we define the reciprocal of the standard deviation (σ) as the SNR of the measurement. In all cases, σ was calculated only in the

Optics EXPRESS

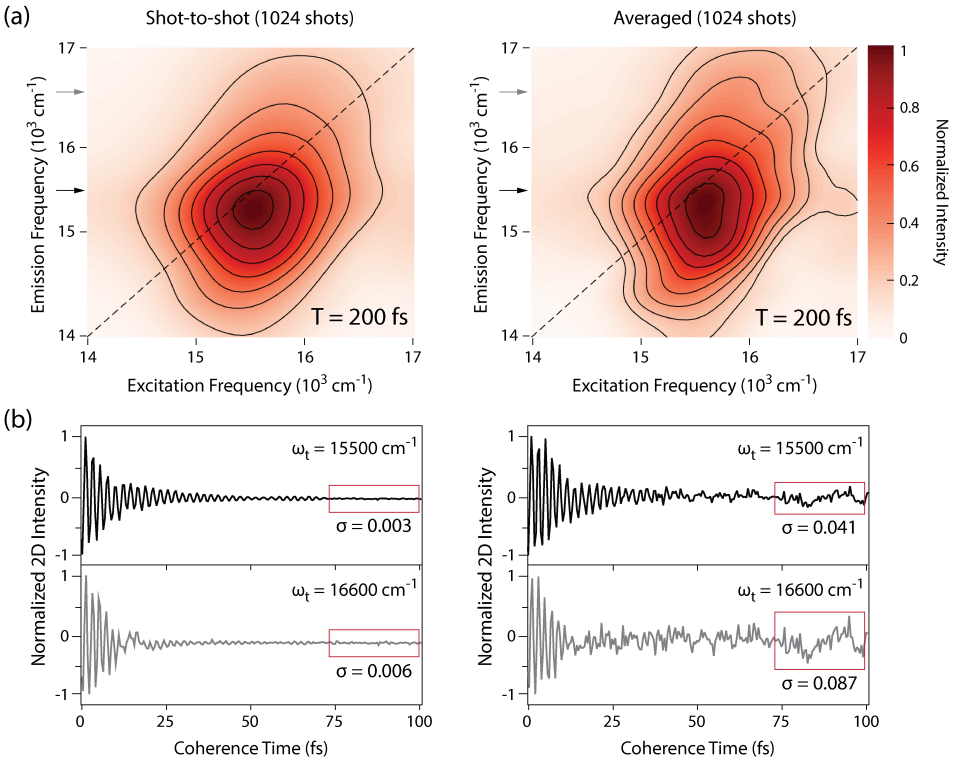

Fig. 8. (a) Comparison of the 2D data of Nile Blue A perchlorate at T = 200 fs acquired with Scheme 1 (left) and Scheme 2 (right), using 1024 laser shots. (b) Normalized raw time-domain signals at emission frequencies of 15500 cm^{-1} (black) and 16600 cm^{-1} (grey) and their noise. The two probed frequencies are marked as arrows in (a). The noise σ was evaluated for $\tau > 75$ fs (marked as red boxes).

range of τ = 75 – 100 fs, where the signal is completely dephased and no oscillatory component remains.

Although the absolute noise level is greater at 16600 cm^{-1} due to the weaker intensity of the 2D signal, Scheme 1 reveals nearly 15-fold improvement in the SNR over Scheme 2 at both frequencies (13.7-fold at ω_t = 15500 cm^{-1}, 14.5-fold at ω_t = 16600 cm^{-1}). These results corroborate that our shot-to-shot acquisition method provides a significant improvement in the sensitivity of detection, which can resolve the instability issue of filamentation-based ultrabroadband light source. Moreover, it can be seen that Scheme 2 fails to resolve the oscillation at τ = 40 – 75 fs, which persists in the shot-to-shot interferogram. This analysis suggests that one would need $(0.041/0.003)^2$ = 187 times more signal averaging with Scheme 2 to acquire 2D data of comparable SNR with that of Scheme 1.

5. Conclusion

We described the construction of an improved 2D electronic spectrometer by combining ultra-broadband pulses generated by gas filamentation with high-speed, shot-to-shot data acquisition. We adopted a dispersion-free method for interferometric control of the coherence time delays, which features high precision as well as a long-term phase stability of $\lambda/75$. We show a 15-fold improvement in sensitivity using our 5-kHz shot-to-shot acquisition scheme while greatly reduc-

Optics EXPRESS

ing the acquisition time, which lays the groundwork for filamentation-based supercontinuum to be extensively employed for broadband 2DES. We envision that the straightforward and robust combination of an ultrabroadband light source and high-sensitivity detection described here will provide us with promising new horizons in 2D spectroscopy, by enabling the detection of previously inaccessible spectroscopic signatures with an extended spectral coverage while maintaining the sensitivity of detection.

Funding

Center for Excitonics (an Energy Frontiers Research Center funded by the U.S. Department of Energy, Office of Science, Office of Basic Energy Sciences) (DE-SC0001088)

Acknowledgments

We would like to thank Drs. John Ogren and Justin Caram for valuable advice on the experimental setup and helpful discussions. We would also like to thank Prof. Gregory Engel for providing the plans for the ARID assembly.